Atmos. Chem. Phys., 22, 14243–14252, 2022
https://doi.org/10.5194/acp-22-14243-2022

Atmospheric Chemistry and Physics
Open Access
EGU

COVID-19 lockdown emission reductions have the potential to explain over half of the coincident increase in global atmospheric methane

David S. Stevenson[1], Richard G. Derwent[2], Oliver Wild[3], and William J. Collins[4]

[1]School of GeoSciences, The University of Edinburgh, Edinburgh, UK
[2]rdscientific, Newbury, UK
[3]Lancaster Environment Centre, Lancaster University, Lancaster, UK
[4]Department of Meteorology, University of Reading, Reading, UK

Correspondence: David S. Stevenson (david.s.stevenson@ed.ac.uk)

Received: 15 July 2021 – Discussion started: 3 August 2021
Revised: 18 October 2022 – Accepted: 20 October 2022 – Published: 8 November 2022

Abstract. Compared with 2019, measurements of the global growth rate of background (marine air) atmospheric methane rose by 5.3 ppb yr^{-1} in 2020, reaching 15.0 ppb yr^{-1}. Global atmospheric chemistry models have previously shown that reductions in nitrogen oxide (NO_x) emissions reduce levels of the hydroxyl radical (OH) and lengthen the methane lifetime. Acting in the opposite sense, reductions in carbon monoxide (CO) and non-methane volatile organic compound (NMVOC) emissions increase OH and shorten methane's lifetime. Using estimates of NO_x, CO, and NMVOC emission reductions associated with COVID-19 lockdowns around the world in 2020 as well as model-derived regional and aviation sensitivities of methane to these emissions, we find that NO_x emission reductions led to a 4.8 (3.8 to 5.8) ppb yr^{-1} increase in the global methane growth rate. Reductions in CO and NMVOC emissions partly counteracted this, changing (reducing) the methane growth rate by −1.4 (−1.1 to −1.7) ppb yr^{-1} (CO) and −0.5 (−0.1 to −0.9) ppb yr^{-1} (NMVOC), yielding a net increase of 2.9 (1.7 to 4.0) ppb yr^{-1}. Uncertainties refer to ±1 standard deviation model ranges in sensitivities. Whilst changes in anthropogenic emissions related to COVID-19 lockdowns are probably not the only important factor that influenced methane during 2020, these results indicate that they have had a large impact and that the net effect of NO_x, CO, and NMVOC emission changes can explain over half of the observed 2020 methane changes. Large uncertainties remain in both emission changes during the lockdowns and methane's response to them; nevertheless, this analysis suggests that further research into how the atmospheric composition changed over the lockdown periods will help us to interpret past methane changes and to constrain future methane projections.

1 Introduction

Methane is a powerful greenhouse gas and an important precursor of tropospheric ozone; both are key air pollutants and short-lived climate forcers (SLCFs). Several factors in addition to rising anthropogenic methane emissions have influenced the evolution of atmospheric methane from its preindustrial level of ∼ 700 ppb to its present-day value of over 1900 ppb. The Intergovernmental Panel on Climate Change's Sixth Assessment Report (Szopa et al., 2021) assessed how changes in emissions of nitrogen oxide (NO_x), carbon monoxide (CO), and non-methane volatile organic compounds (NMVOCs) have contributed to historical changes in methane via their impacts on OH, the main sink for methane. A range of modelling studies have explored these indirect impacts on methane (e.g. Shindell et al., 2005, 2009; Stevenson et al., 2013; Thornhill et al., 2021). For example, the Atmospheric Chemistry and Climate Model Intercomparison Project found that 1850–2000 increases in anthropogenic NO_x emissions had reduced year 2000 methane levels by 955 ppb, whilst growing emissions of CO and NMVOCs had increased methane by 150 and 59 ppb respectively (Table 7

of Stevenson et al., 2013). These results have quite large uncertainties (at least ±10 %, based on the model range in Stevenson et al., 2013) but indicate that non-methane (especially NO_x) emissions have had very significant impacts on methane. Better understanding of what controls methane and its evolution is vital for progress towards the Paris Climate Agreement target that seeks to limit warming to 1.5 °C above pre-industrial levels.

Following the onset of the COVID-19 pandemic in early 2020, the trace gas composition of the global atmosphere changed substantially. Atmospheric NO_x levels decreased as surface and aviation NO_x emissions fell (Bauwens et al., 2020; Cooper et al., 2022), whilst the measured growth rate of methane (CH_4) rose sharply in 2020 (Laughner et al., 2021). The observed NO_x changes are clearly linked to falls in emissions resulting from lockdowns, but the driver of the methane increases is less clear, with some studies discussing causes related to decreases in OH (e.g. Weber et al., 2020; Laughner et al., 2021), whereas others suggest rises in sources (e.g. Feng et al., 2022). Methane, NO_x, CO, and NMVOCs are linked via the oxidising capacity of the atmosphere, specifically by the abundance of the hydroxyl (OH) radical. The response of global atmospheric chemistry to the large lockdown perturbation since early 2020 provides an opportunity to explore the sensitivity of the NO_x–CO–NMVOC–OH–CH_4 system and to compare models and observations. Here, we use model-derived sensitivities of global methane to NO_x, CO, and NMVOC emissions as well as the estimated changes in anthropogenic emissions of these species related to the COVID-19 lockdowns to calculate estimated impacts from lockdown emission changes on the growth rate of global methane, and we compare this to observations.

2 Measurements of atmospheric methane and nitrogen oxides

Recent methane measurements from the US National Oceanographic and Atmospheric Administration (NOAA) show that the atmospheric (marine air background) methane growth rate rose sharply from 9.7 ppb yr^{-1} in 2019 to 15.0 ppb yr^{-1} in 2020, higher than any preceding annual value in the NOAA record, which started in 1984 (Dlugokencky, 2022). Many of the earlier large year-to-year jumps in methane's growth rate relate in part to variability in climate and emissions associated with the El Niño–Southern Oscillation (ENSO) and in part to modulation of methane's main sink, oxidation by OH (Turner et al., 2018; Zhao et al., 2020). The start of 2020 marked the onset of a La Niña that has persisted into 2022. Past La Nina phases have not always shown clear links with methane's growth rate, and the influence of the current ENSO phase on methane is uncertain.

Measurements of nitrogen dioxide (NO_2) from satellite instruments and nitrogen monoxide (NO) and NO_2 from surface sites show that the levels of atmospheric NO_x ($NO + NO_2$) dramatically fell globally during 2020 (Bauwens et al., 2020; Laughner et al., 2021; Cooper et al., 2022). This was driven by COVID-19 lockdowns around the world that reduced emissions, mainly from transportation (Venter et al., 2020; Lamboll et al., 2021; Doumbia et al., 2021).

3 Sensitivity of global methane to NO_x, CO, and NMVOC emissions

Global atmospheric chemistry model simulations indicate that decreases in NO_x emissions lead to reductions in OH and increases in the global methane lifetime (Prather, 1994; Derwent et al., 2001; Wild et al., 2001; Stevenson et al., 2004; Weber et al., 2020). Similarly, decreases in CO and NMVOC emissions lead to increases in OH and decreases in the methane lifetime (Derwent et al., 2001; Wild et al., 2001). Although methane has an atmospheric lifetime of about 10 years, models show that its peak response occurs within a few months of the cessation of a sudden short-lived (month- or year-long) pulse of extra emissions (Derwent et al., 2001; Wild et al., 2001; Stevenson et al., 2004). This indicates that the impacts on methane from the sudden changes in emissions associated with lockdowns will have had rapid impacts on methane's growth rate.

We first illustrate the basis of our approach by describing the model experiments performed by Derwent et al. (2001), who conducted a series of simulations with the global tropospheric chemistry model STOCHEM to quantify the impact of NO_x emissions on methane. They compared a 4-year-long base simulation with a perturbation simulation that was identical apart from an enhancement in NO_x emissions of magnitude 1 Tg(NO_2), added during the first month with the Northern Hemisphere surface anthropogenic NO_x emission distribution. The extra NO_x produced a short-lived increase in OH, and this led to a rapid depletion of global methane, which peaked with a magnitude of around 0.39 Tg(CH_4) after about 6 months. The methane deficit then exponentially decayed with an e-folding timescale of about 12 years (the methane perturbation lifetime, τ), with methane levels returning towards their base values. Wild et al. (2001) conducted similar experiments, with year-long emission perturbations using a different model (UCI CTM), and they found very similar behaviour but with slightly larger sensitivities: 1 Tg(NO_2) from global fossil fuel sources yielded a 0.55 Tg depletion of CH_4. These studies also investigated the impact of CO and NMVOC emissions. Changes in the global methane burden (Tg) are converted to changes in the tropospheric mole fraction (ppb) using the total atmosphere mass of 5.113×10^9 Tg and a fill factor of 0.973 for conversion of a total atmosphere abundance to a tropospheric abundance (Prather et al., 2012). We assume the troposphere is well mixed, so surface changes will be the same as whole troposphere changes.

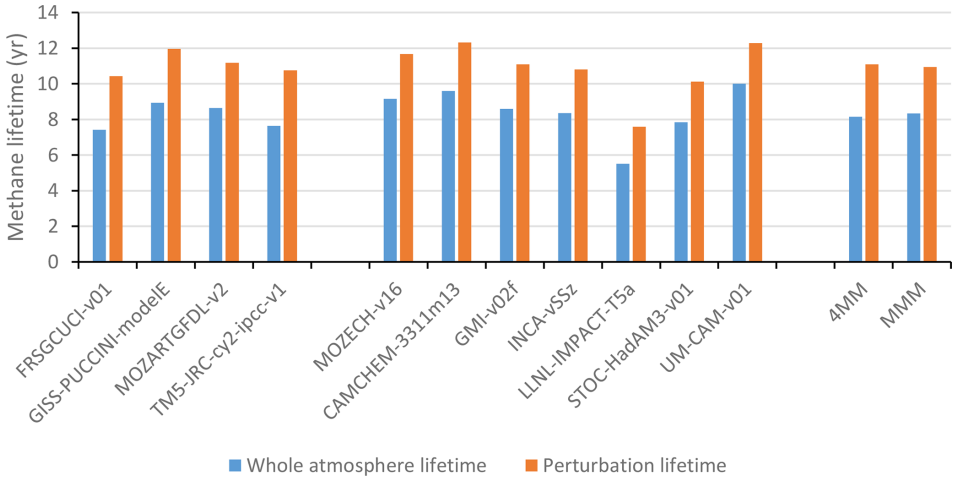

Figure 1. Whole-atmosphere and perturbation methane lifetimes (in years, blue) for the Hemispheric Transport of Air Pollutants (HTAP) models as well as the four-model mean (4MM) of the core models (four models on the left) and the multi-model mean (MMM). The perturbation lifetime was derived from 20 % methane reduction experiments (orange; see Table S4).

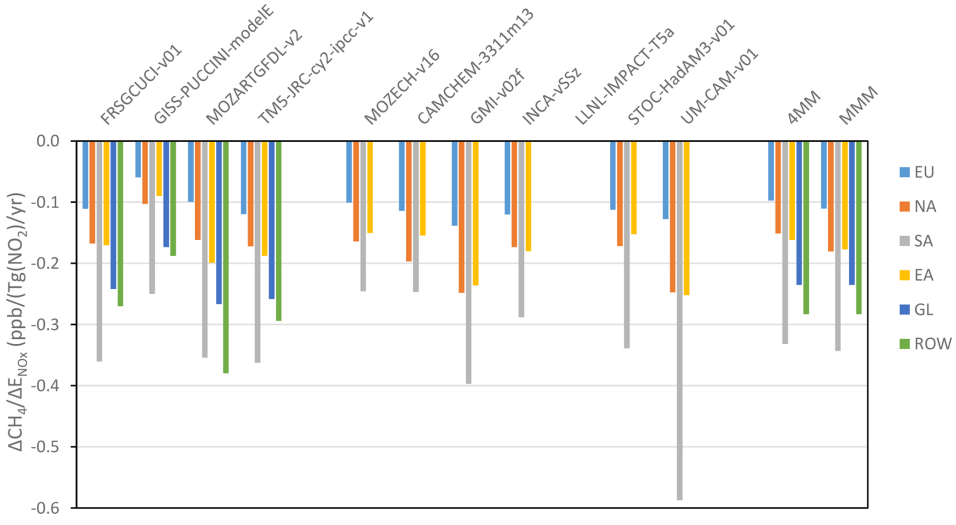

Figure 2. Sensitivity of global methane (ppb) to changes in anthropogenic NO_x emissions ($Tg(NO_2)\,yr^{-1}$), derived from 20 % reduction experiments performed by the HTAP models for four regions (Europe, EU; North America, NA; South Asia, SA; and East Asia, EA), globally (GL), and for the ROW (everywhere outside of the four HTAP regions). Global (and hence ROW) results are only available for the four core models, shown on the left of the figure. Also shown are the 4MM and MMM. There are no results for the LLNL-IMPACT-T5a model for NO_x; it is included to maintain consistency with Figs. 3 and 4.

More recently, Fry et al. (2012) analysed results from 11 global models that took part in the Hemispheric Transport of Air Pollutants (HTAP) study in order to isolate the impacts of anthropogenic NO_x, CO, and NMVOC emissions from Europe (EU), North America (NA), South Asia (SA), and East Asia (EA) on methane. We utilise that ensemble of model results here; model descriptions are given in Fiore et al. (2009). Models performed a base simulation as well as a series of further repeat simulations with 20 % lower anthropogenic emissions for each species for each region. In addition to the 20 % regional emission reduction experiments, some models also performed global 20 % emission reduction experiments (Wild et al., 2012). The results from Fry et al. (2012) and Wild et al. (2012) and the details of our analysis are presented in the Supplement. Four models include results from all of the regional and global perturbation simulations: FRSGCUCI-v01, GISS-PUCCINI-modelE, MOZARTGFDL-v2, and TM5-JRC-cy2-ipcc-v1. We calculate a "four-model mean" (4MM) based on these model results. We also show results from the other models to illustrate the range of model behaviour as well as providing "multi-model mean" (MMM) results from all available simulations.

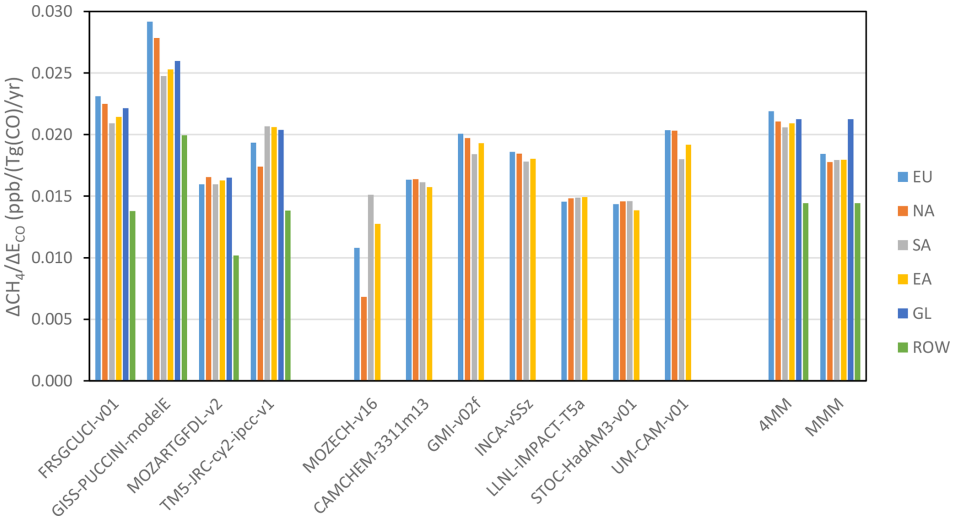

Figure 3. As in Fig. 2 but showing methane sensitivities for changes in surface anthropogenic CO emissions (Tg(CO) yr^{-1}).

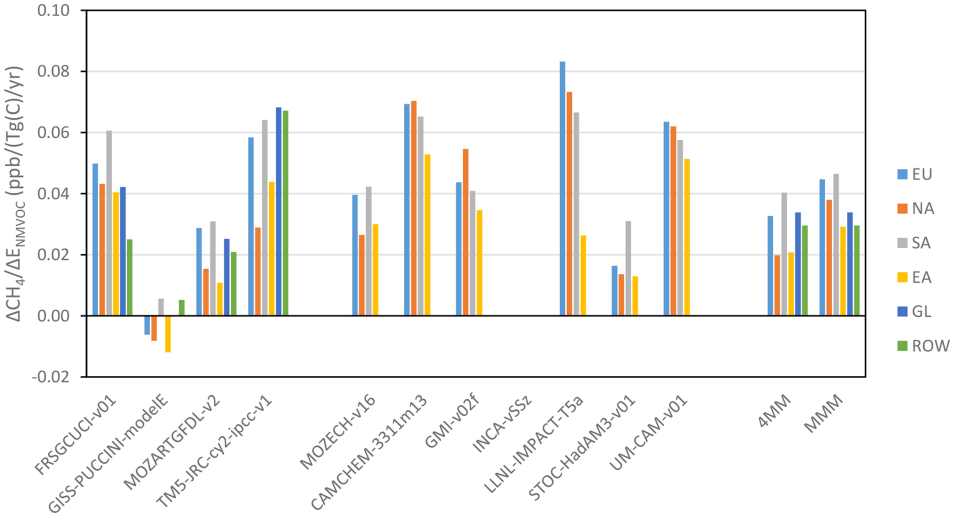

Figure 4. As in Fig. 2 but showing methane sensitivities for changes in surface anthropogenic NMVOC emissions (Tg(C) yr^{-1}). There are no results for the INCA-vSSz model for NMVOCs.

In the HTAP simulations, methane was fixed as a prescribed boundary condition, precluding direct diagnosis of changes in methane. However, methane changes can be diagnosed indirectly by analysing the methane lifetime associated with the tropospheric OH sink in each run. We convert these to whole-atmosphere lifetimes by assuming fixed lifetimes for methane losses to soils (150 years), reaction with chlorine radicals (200 years), and in the stratosphere (120 years) (Prather et al., 2012). The HTAP experiments also included a global methane perturbation simulation – allowing the methane feedback factor and perturbation lifetime to be calculated (Prather, 1994; Holmes, 2018). Figure 1 shows whole-atmosphere and perturbation methane lifetimes for the HTAP models, with MMM values of 8.3 and 10.9 years respectively.

Differences between simulations yielded the change in methane lifetimes due to changes in regional/global emissions. From these changes in methane lifetime, the equilibrium change in methane was calculated – that is, the change in methane that would have occurred if methane levels had been free to respond (e.g. see Stevenson et al., 2013). In model simulations where methane is not prescribed, methane adjusts towards equilibrium with an *e*-folding timescale given by its perturbation lifetime (Derwent et al., 2001; Wild et al., 2001; Holmes, 2018). We convert equilibrium methane changes derived from sustained changes in emissions to the equivalent methane response for a pulse of emissions for each experiment. We use each model's perturbation lifetime to calculate the fraction of the equilibrium response that would have been reached after 1 year; for example, for the

Table 1. Changes in global and regional annual anthropogenic emissions from 2019 to 2020 (in Tg and as a percentage of 2019) assumed to be associated with COVID-19 lockdowns. The rest of the world (ROW) is defined as everywhere apart from the four HTAP regions. Derived from data in Lamboll et al. (2021).

	Surface NO_x		Aviation NO_x		Surface CO		Surface NMVOCs	
	$Tg(NO_2)$	%	$Tg(NO_2)$	%	Tg(CO)	%	Tg(C)	%
Global emissions (GL)	−19.38	*−14.6*	−0.83	*−23.2*	−73.38	*−12.9*	−15.65	*−9.9*
Europe (EU)	−2.65	*−15.8*	−0.23	*−23.4*	−6.09	*−18.1*	−1.71	*−10.7*
North America (NA)	−2.55	*−18.7*	−0.23	*−23.1*	−7.49	*−14.0*	−1.56	*−12.3*
South Asia (SA)	−3.78	*−16.5*	−0.02	*−23.0*	−16.76	*−16.1*	−4.34	*−16.1*
East Asia (EA)	−4.40	*−11.8*	−0.08	*−22.9*	−24.58	*−12.5*	−2.41	*−6.5*
Rest of the world (ROW)	−6.00	*−14.3*	−0.28	*−23.1*	−18.46	*−18.5*	−5.63	*−8.6*

multi-model mean (MMM) methane perturbation lifetime of 10.9 years (Fig. 1), this fraction is $(1\text{-}e^{-1/\tau}) = 8.8\,\%$. This method is appropriate because we undertake a comparison to changes in the observed annual growth rate, and it is justified by the rapid response of global methane seen in transient model simulations where methane is free to respond, as well as by the fact that the largest lockdown emission perturbations occurred in the first half of 2020. We normalise results to produce global methane sensitivities per teragram of gas emitted for each HTAP region and globally for each model. Figures 2, 3, and 4 show global methane sensitivities for NO_x, CO, and NMVOC emissions respectively.

Figure 2 shows relatively consistent responses to NO_x emissions, with all models least sensitive to EU NO_x emissions and most sensitive to SA emissions, with NA and EA emissions being in between. Global and ROW sensitivities are relatively high. The 4MM sensitivities are slightly lower than those for the MMM.

Figure 3 shows relatively consistent behaviour across the models for CO, with less variation between regions, reflecting the longer lifetime of CO, which makes the location of emissions less important. The ROW sensitivities, inferred from the global results, are relatively low. The 4MM sensitivities for CO are slightly larger than the MMM values.

Figure 4 shows more divergence in the model response to NMVOC emissions, with one model (GISS-PUCCINI-modelE) displaying an opposite sensitivity to the other models (apart from for SA and ROW emissions) and some models showing quite large sensitivities whilst others are small. This probably reflects the differing methods of representing NMVOCs in each model, in terms of the number of species, the grouping together of species, and the sophistication of their oxidation chemistry. Somewhat fortuitously, the 4MM and MMM are similar.

The HTAP experiments used 2001 as their base year, prescribing global methane to be 1760 ppb, and each model used their own best estimates of global 2001 emissions. In 2020, surface-level background global mean methane was ~ 1870 ppb, and emissions of NO_x, CO, and NMVOCs had changed relative to 2001. Sensitivities of methane to emissions derived from the HTAP results will differ somewhat from those that would be found if 2020 conditions were used, and this represents an important caveat to our results. However, these differences are unlikely to be substantial, and no more up-to-date multi-model study of the impacts of regional NO_x, CO, and NMVOC emissions on methane has been published to date, so it represents our best source of information in the literature.

The HTAP perturbation experiments were for all anthropogenic emissions, including aviation, which is a significant NO_x source. Similar model simulations have calculated the sensitivity of methane to aviation NO_x emissions, and this allows us to separate out the effects from aviation. Wild et al. (2001) and Stevenson et al. (2004) conducted NO_x pulse experiments, adding NO_x using the global aviation NO_x emission distribution, and found a peak impact on global methane of about 2.5–2.6 Tg (equivalent to mole fractions of 0.88–0.92 ppb) for a 1 $Tg(NO_2)$ emission perturbation. Stevenson and Derwent (2009) also found spatial variation in sensitivity for aviation NO_x, with the more sensitive regions tending to have lower background NO_x levels. The most up-to-date study of aviation NO_x is Lee et al. (2021), who assessed multi-model results using sustained emission changes, similarly to the HTAP study. Lee et al. (2021) report a methane radiative forcing sensitivity to aviation NO_x emissions of $-15.8\,mW\,m^{-2}\,(Tg(N)\,yr^{-1})^{-1}$ (their Table 3). We convert this to a methane mole fraction sensitivity to NO_x emissions using the relationship between changes in the mole fraction and radiative forcing given by Myhre et al. (1998); using a similar methodology to that described above, we then convert the product to the equivalent response for a pulse of emissions. This yields a sensitivity of methane to a pulse change in aviation NO_x emissions of 1.12 ppb $(CH_4)/Tg(NO_2)\,yr^{-1}$, which is similar to, although slightly higher than, results from earlier studies. Lee et al. (2021) also report a 95 % likelihood range on the radiative forcing sensitivity, which translates to a standard deviation of 0.21 ppb $(CH_4)/Tg(NO_2)\,yr^{-1}$, which we take to be a representative uncertainty for the mole fraction sensitivity to aviation NO_x emissions.

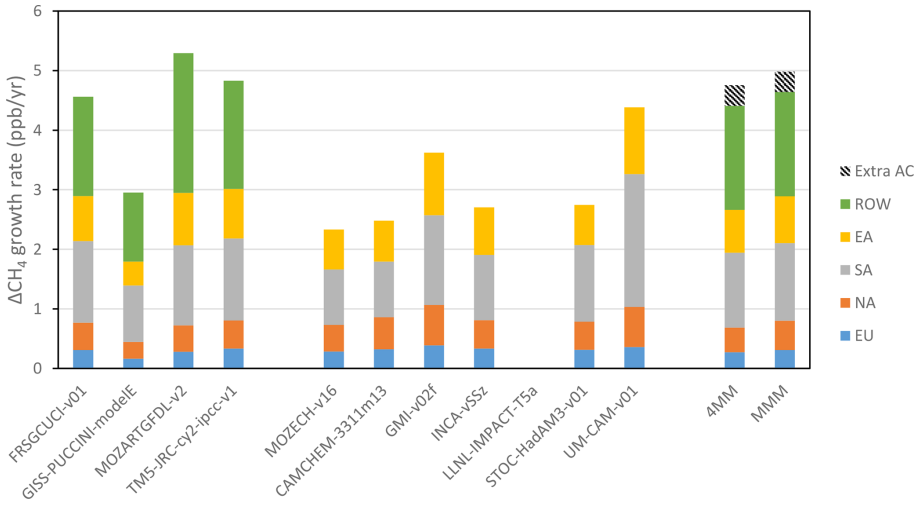

Figure 5. Calculated changes in the global methane growth rate from changes in anthropogenic NO_x emissions during the 2020 lockdown for each of the HTAP models. Also shown are values for the mean of the four core models (shown on left) (4MM) that reported results for all simulations as well as multi-model mean (MMM) results based on all available models. The four core models included global experiments, allowing the calculation of ROW contributions. Regional contributions partially include aviation NO_x; a further contribution from aviation (Extra AC) is also shown for the multi-model results (see the text for details).

Table 2. Summary of impacts on the 2020 global methane growth rate (ppb yr^{-1}) relative to 2019 due to COVID-19 lockdown emission reductions based on 4MM results. Values for total aviation NO_x are given in parentheses, as they are already partly included in the regional values; the additional aviation component not included in the regional values (Aviation (extra)) is also shown.

	NO*x*	CO	NMVOCs	Total
EU	0.27 ± 0.07	-0.13 ± 0.03	-0.06 ± 0.05	0.08 ± 0.10
NA	0.41 ± 0.09	-0.16 ± 0.04	-0.03 ± 0.03	0.22 ± 0.10
SA	1.26 ± 0.21	-0.34 ± 0.06	-0.17 ± 0.12	0.74 ± 0.25
EA	0.72 ± 0.22	-0.51 ± 0.09	-0.05 ± 0.06	0.15 ± 0.25
ROW	1.75 ± 0.49	-0.27 ± 0.07	-0.17 ± 0.15	1.31 ± 0.51
Aviation (extra)	0.34 ± 0.06			0.34 ± 0.06
Aviation (total)	(0.93 ± 0.18)			(0.93 ± 0.18)
Total	4.75 ± 1.02	-1.42 ± 0.29	-0.48 ± 0.39	2.86 ± 1.13

4 COVID-19 lockdown impacts on emissions

Lamboll et al. (2021) compiled estimates of the impact of COVID-19 lockdowns on global anthropogenic NO_x, CO, and NMVOC emissions, as monthly mean time series with a spatial resolution of $0.5° \times 0.5°$ (latitude $\times$ longitude). We use these data to calculate the difference in surface and aviation NO_x emissions between 2019 (pre-lockdown) and 2020 for the four HTAP regions as well as globally and, hence, for the "rest of the world" (ROW) region (i.e. everywhere beyond the four HTAP regions). The annual reduction in global surface NO_x emissions from 2019 to 2020 was about 19.38 Tg(NO_2), or 15 %. Lamboll et al. (2021) also compiled data on aviation emissions, estimating a global reduction of about 0.83 Tg(NO_2), or 23 %. Global and regional annual changes in NO_x, CO, and NMVOC emissions are summarised in Table 1.

5 Impacts of reduced lockdown emissions on global methane

To calculate an approximate impact of the lockdown emission reductions on global methane, we simply multiply the regional/aviation sensitivities and emission changes and sum over the globe. To calculate ROW contributions, we assume that the global sensitivity values can be linearly constructed from the four regions and the ROW, weighting each region by its emissions.

An additional complication is that the regional sensitivities from HTAP for anthropogenic NO_x emissions (shown in Fig. 2) are for a combination of surface and aviation sources. The percentage changes in emissions related to lockdowns for surface and aviation NO_x emissions differ (Table 1). We first calculate contributions to the global change in methane using the regional sensitivities derived from HTAP (Fig. 2)

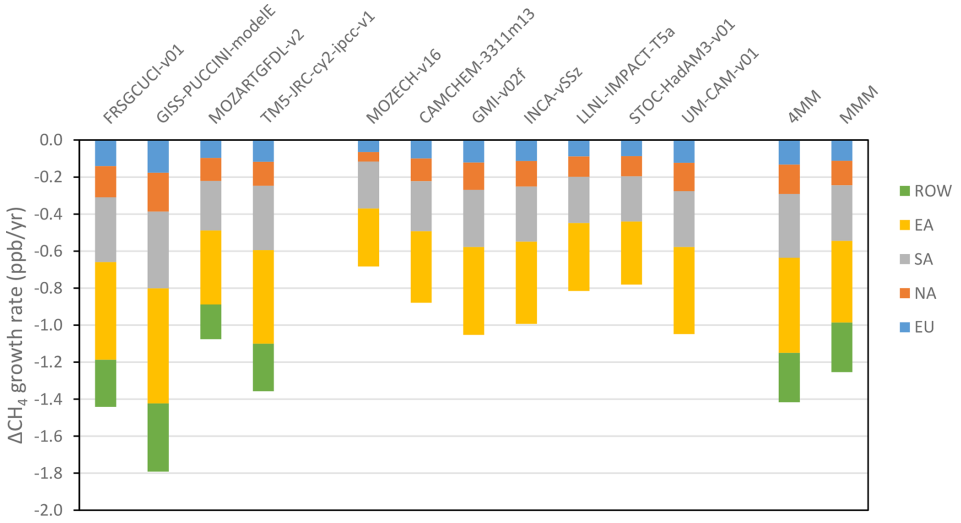

Figure 6. As in Fig. 5 but for CO emissions.

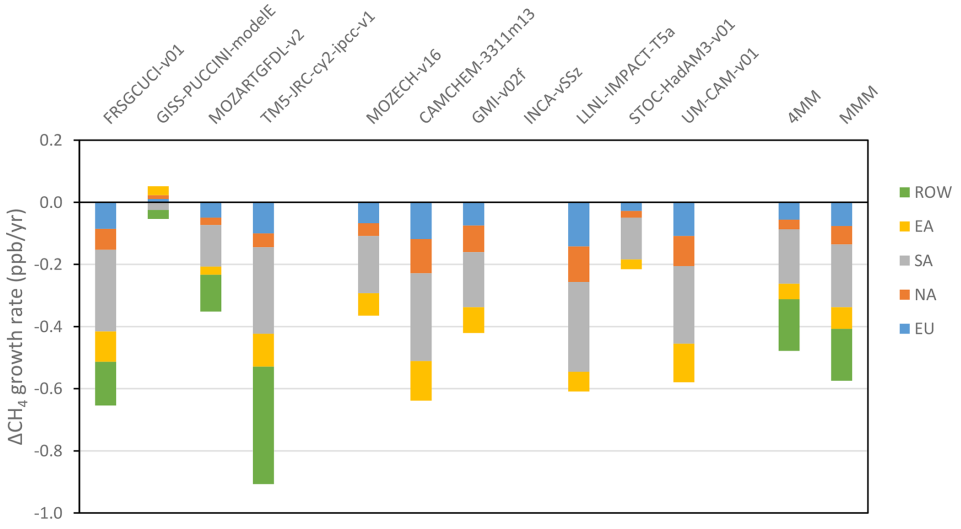

Figure 7. As in Fig. 5 but for NMVOC emissions.

in order to account for the changes in regional surface emissions. For example, for Europe, surface NO_x emissions decreased by 2.65 Tg(NO_2), or 15.8 %. By using this 15.8 % reduction with the EU sensitivity, we account for an annual 15.8 % reduction in aviation NO_x emissions (0.15 Tg(NO_2)) from the region. However, the total change in aviation NO_x emissions over Europe is 23.4 %, or 0.23 Tg(NO_2), so another 0.08 Tg(NO_2) needs to be included. Globally, another 0.31 Tg(NO_2) needs to be added (Table S11b) in addition to that already accounted for using the HTAP regional sensitivities. We use the global sensitivity to aviation NO_x emissions derived from Lee et al. (2021) (1.12 ± 0.21 ppb (CH_4)/Tg(NO_2) yr^{-1}; see Sect. 3) with this value to derive an extra aviation component of 0.34 ± 0.06 ppb (CH_4) (Fig. 5, Table 2).

Figure 5 shows the calculated contributions to the global methane growth rate from changes in NO_x emissions for each of the HTAP models as well as the 4MM and MMM values. Equivalent results for CO and NMVOCs are shown in Figs. 6 and 7 respectively. Table 2 summarises the regional and aviation components for all emissions, using results from the 4MM.

We find that reduced NO_x emissions during lockdown increased the methane growth rate in total by 4.8 ± 1.0 ppb yr^{-1} (4MM; a slightly larger impact of 5.0 ± 1.0 ppb yr^{-1} is found for the MMM). South Asia is the largest contributing HTAP region, although this is exceeded by the impact from NO_x emission changes from outside of the four HTAP regions. Aviation NO_x is also an important contributor, making up about one-fifth of the total from NO_x. Reduced CO emis-

sions partly counteracted this positive impact on the methane growth rate, with an overall impact of -1.4 ± 0.3 ppb yr^{-1} (4MM; a slightly smaller impact of -1.3 ± 0.3 ppb yr^{-1} is found for the MMM). East Asia is the largest contributing region, followed by South Asia. Reduced NMVOC emissions had an additional effect in the same sense as CO, although about one-third smaller and with a larger uncertainty. The overall impact from NMVOCs was -0.5 ± 0.4 ppb yr^{-1} (4MM; slightly larger value of -0.6 ± 0.4 ppb yr^{-1} is found for the MMM).

We find a net total impact on methane of 2.9 ± 1.1 ppb yr^{-1} (4MM; 3.2 ± 1.1 ppb yr^{-1} is found for the MMM), with the largest contributing region overall being ROW, followed by South Asia. Aviation NO_x changes make up about 30 % of this net total.

6 Discussion and conclusions

These model-derived results can be compared to the observed increase in the methane growth rate from 2019 to 2020 of 5.3 ppb yr^{-1}, and they suggest that lockdown emission changes in NO_x, CO, and NMVOCs can explain 54 % ± 21 % (4MM; 60 % ± 21 % is found for the MMM) of this increase. Uncertainties are standard deviations of the HTAP (Fry et al., 2012) and aviation NO_x (Lee et al., 2021) models' sensitivity ranges. No uncertainty estimate is included here for the magnitude of lockdown emission changes, which is probably similar in magnitude. Our results have several important caveats, and refinements to this relatively simply derived estimate will need to account for a number of additional complications. The emission changes have temporal structure (Lamboll et al., 2021), as do the sensitivities of methane to NO_x, CO, and NMVOCs, and these will interact. One study has reported a reduction in lightning during 2020 (Vasquez, 2022), which may contribute much like reductions in aircraft NO_x. The regional sensitivities derived here are based on emission changes with the spatial distributions and base magnitudes of the 2001 anthropogenic emissions, rather than a 2020 emission baseline and the actual changes during lockdown. Given the non-linearities in the response of OH to emissions, the real sensitivities are likely to be slightly different to those calculated here, and this increases the uncertainty in our results. Detailed modelling of the lockdown period is starting to explore these effects (Weber et al., 2020; Miyazaki et al., 2021). There is also spatio-temporal structure in the observed methane changes (e.g. Laughner et al., 2021; Feng et al., 2022) that will yield further information. There are undoubtedly several other factors, in addition to changes in anthropogenic NO_x, CO, and NMVOC emissions that influenced methane during 2020. Nevertheless, it seems likely that the dramatic reductions in these emissions, especially NO_x, brought about by the COVID-19 lockdowns can explain a large component of the surge in the methane growth rate seen during 2020. These influences on methane related to changes in OH need to be carefully accounted for in any attribution study that attempts to explain the recent observed dramatic changes in methane.

Code and data availability. The original data used here are all freely accessible in the cited references: Fiore et al. (2009, https://doi.org/10.1029/2008JD010816), Fry et al. (2012, https://doi.org/10.1029/2011JD017134), Wild et al. (2012, https://doi.org/10.5194/acp-12-2037-2012), Lamboll et al. (2021, https://doi.org/10.5194/gmd-14-3683-2021), and Lee et al. (2021, https://doi.org/10.1016/j.atmosenv.2020.117834). All calculations are detailed in the Supplement.

Supplement. The supplement related to this article is available online at: https://doi.org/10.5194/acp-22-14243-2022-supplement.

Author contributions. DSS wrote the text and performed the main analysis. OW and WJC performed additional analysis and commented on the text. RGD commented on the text.

Competing interests. The contact author has declared that none of the authors has any competing interests.

Disclaimer. Publisher's note: Copernicus Publications remains neutral with regard to jurisdictional claims in published maps and institutional affiliations.

Acknowledgements. We acknowledge all of the modellers who contributed results to the HTAP phase 1 study; without those results, this work would not have been possible. Jize Jiang is thanked for his technical help with the analysis.

Financial support. This work was partly supported by the Natural Environment Research Council (grant no. NE/S009019/1) and the Royal Society (grant no. IES_R3_193183).

Review statement. This paper was edited by Andreas Hofzumahaus and reviewed by three anonymous referees.

References

Bauwens, M., Compernolle, S., Stavrakou, T., Müller, J.-F., van Gent, J., Eskes, H., Levelt, P. F., van der A, R., Veefkind, J. P., Vlietinck, J., Yu, H., and Zehner, C.: Impact of coronavirus outbreak on NO_2 pollution assessed using TROPOMI and OMI observations, Geophys. Res. Lett., 47, e2020GL087978, https://doi.org/10.1029/2020GL087978, 2020.

Cooper, M. J., Martin, R. V., Hammer, M. S., Levelt, P. F., Veefkind, P., Lamsal, L. N., Krotkov, N. A., Brook, J. R.,

and McLinden, C. A.: Global fine-scale changes in ambient NO_2 during COVID-19 lockdowns, Nature, 601, 380–387, https://doi.org/10.1038/s41586-021-04229-0, 2022.

Derwent, R. G., Collins, W. J., Johnson, C. E., and Stevenson, D. S.: Transient Behaviour of Tropospheric Ozone Precursors in a Global 3-D CTM and Their Indirect Greenhouse Effects, Clim. Change, 49, 463–487, https://doi.org/10.1023/A:1010648913655, 2001.

Dlugokencky, E.: NOAA/GML Trends in Atmospheric Methane, https://gml.noaa.gov/ccgg/trends_ch4/, last access: 16 September 2022.

Doumbia, T., Granier, C., Elguindi, N., Bouarar, I., Darras, S., Brasseur, G., Gaubert, B., Liu, Y., Shi, X., Stavrakou, T., Tilmes, S., Lacey, F., Deroubaix, A., and Wang, T.: Changes in global air pollutant emissions during the COVID-19 pandemic: a dataset for atmospheric modeling, Earth Syst. Sci. Data, 13, 4191–4206, https://doi.org/10.5194/essd-13-4191-2021, 2021.

Feng, L., Palmer, P. I., Parker, R. J., Lunt, M. F., and Boesch, H.: Methane emissions responsible for record-breaking atmospheric methane growth rates in 2020 and 2021, Atmos. Chem. Phys. Discuss. [preprint], https://doi.org/10.5194/acp-2022-425, in review, 2022.

Fiore, A. M., Dentener, F. J., Wild, O., Cuvelier, C., Schultz, M. G., Hess, P., Textor, C., Schulz, M., Doherty, R. M., Horowitz, L. W., MacKenzie, I. A., Sanderson, M. G., Shindell, D. T., Stevenson, D. S., Szopa, S., Van Dingenen, R., Zeng, G., Atherton, C., Bergmann, D., Bey, I., Carmichael, G., Collins, W. J., Duncan, B. N., Faluvegi, G., Folberth, G., Gauss, M., Gong, S., Hauglustaine, D., Holloway, T., Isaksen, I. S. A., Jacob, D. J., Jonson, J. E., Kaminski, J. W., Keating, T. J., Lupu, A., Marmer, E., Montanaro, V., Park, R. J., Pitari, G., Pringle, K. J., Pyle, J. A., Schroeder, S., Vivanco, M. G., Wind, P., Wojcik, G., Wu, S., and Zuber, A.: Multimodel estimates of intercontinental source-receptor relationships for ozone pollution, J. Geophys. Res., 114, D04301, https://doi.org/10.1029/2008JD010816, 2009.

Fry, M. M., Naik, V., West, J. J., Schwarzkopf, M. D., Fiore, A. M., Collins, W. J., Dentener, Frank J., Shindell, D. T., Atherton, C., Bergmann, D., Duncan, B. N., Hess, P., MacKenzie, I. A., Marmer, E., Schultz, M. G., Szopa, S., Wild, O., and Zeng, G.: The influence of ozone precursor emissions from four world regions on tropospheric composition and radiative climate forcing, J. Geophys. Res., 117, D07306, https://doi.org/10.1029/2011JD017134, 2012.

Holmes, C. D.: Methane feedback on atmospheric chemistry: Methods, models, and mechanisms, J. Adv. Model. Earth Syst., 10, 1087–1099, https://doi.org/10.1002/2017MS001196, 2018.

Lamboll, R. D., Jones, C. D., Skeie, R. B., Fiedler, S., Samset, B. H., Gillett, N. P., Rogelj, J., and Forster, P. M.: Modifying emissions scenario projections to account for the effects of COVID-19: protocol for CovidMIP, Geosci. Model Dev., 14, 3683–3695, https://doi.org/10.5194/gmd-14-3683-2021, 2021.

Laughner, J. L., Neu, J. L., Schimel, D., Wennberg, P. O., Barsanti, K., Bowman, K. W., Chatterjee, A., Croes, B. E., Fitzmaurice, H. L., Henze, D. K., Kim, J., Kort, E. A., Liu, Z., Miyazaki, K., Turner, A. J., Anenberg, S., Avise, J., Cao, H., Crisp, D., de Gouw, J., Eldering, A., Fyfe, J. C., Goldberg, D. L., Gurney, K. R., Hasheminassab, S., Hopkins, F., Ivey, C. E., Jones, D. B. A., Liu, J., Lovenduski, N. S., Martin, R. V., McKinley, G. A., Ott, L., Poulter, B., Ru, M., Sander, S. P., Swart, N., Yung, Y. L., and Zeng, Z.-C.: Societal shifts due to COVID-19 reveal large-scale complexities and feedbacks between atmospheric chemistry and climate change, P. Natl. Acad. Sci. USA, 118, e2109481118, https://doi.org/10.1073/pnas.2109481118, 2021.

Lee, D. S., Fahey, D. W., Skowron, A., Allen, M. R., Burkhardt, U., Chen, Q., Doherty, S. J., Freeman, S., Forster, P. M., Fuglestvedt, J., Gettelman, A., De León, R. R., Lim, L. L., Lund, M. T., Millar, R. J., Owen, B., Penner, J. E., Pitari, G., Prather, M. J., Sausen, R., and Wilcox, L. J.: The contribution of global aviation to anthropogenic climate forcing for 2000 to 2018, Atmos. Environ., 244, 117834, https://doi.org/10.1016/j.atmosenv.2020.117834, 2021.

Miyazaki, K., Bowman, K., Sekiya, T., Takigawa, M., Neu, J. L., Sudo, K., Osterman, G., and Eskes, H.: Global tropospheric ozone responses to reduced NO_x emissions linked to the COVID-19 worldwide lockdowns, Sci. Adv., 7, eabf7460, https://doi.org/10.1126/sciadv.abf7460, 2021.

Myhre, G., Highwood, E., Shine, K., and Stordal, F.: New estimates of radiative forcing due to well mixed greenhouse gases, Geophys. Res. Lett., 25, 2715–2718, https://doi.org/10.1029/98GL01908, 1998.

Prather, M. J.: Lifetimes and Eigenstates in Atmospheric Chemistry, Geophys. Res. Lett., 21, 801–804, 1994.

Prather, M. J., Holmes, C. D., and Hsu, J.: Reactive greenhouse gas scenarios: Systematic exploration of uncertainties and the role of atmospheric chemistry, Geophys. Res. Lett., 39, L09803, https://doi.org/10.1029/2012GL051440, 2012.

Shindell, D. T., Faluvegi, G., Bell, N., and Schmidt, G. A.: An emissions-based view of climate forcing by methane and tropospheric ozone, Geophys. Res. Lett., 32, L04803, https://doi.org/10.1029/2004GL021900, 2005.

Shindell, D. T., Faluvegi, G., Koch, D. M., Schmidt, G. A., Unger, N., and Bauer, S. E.: Improved attribution of climate forcing to emissions, Science, 326, 716–718, https://doi.org/10.1126/science.1174760, 2009.

Stevenson, D. S. and Derwent, R. G.: How does the location of aircraft nitrogen oxide emissions affect their climate impact?, Geophys. Res. Lett., 36, L17810, https://doi.org/10.1029/2009GL039422, 2009.

Stevenson, D. S., Doherty, R. M., Sanderson, M. G., Collins, W. J., Johnson, C. E., and Derwent, R. G.: Radiative forcing from aircraft NO_x emissions: Mechanisms and seasonal dependence, J. Geophys. Res., 109, D17307, https://doi.org/10.1029/2004JD004759, 2004.

Stevenson, D. S., Young, P. J., Naik, V., Lamarque, J.-F., Shindell, D. T., Voulgarakis, A., Skeie, R. B., Dalsoren, S. B., Myhre, G., Berntsen, T. K., Folberth, G. A., Rumbold, S. T., Collins, W. J., MacKenzie, I. A., Doherty, R. M., Zeng, G., van Noije, T. P. C., Strunk, A., Bergmann, D., Cameron-Smith, P., Plummer, D. A., Strode, S. A., Horowitz, L., Lee, Y. H., Szopa, S., Sudo, K., Nagashima, T., Josse, B., Cionni, I., Righi, M., Eyring, V., Conley, A., Bowman, K. W., Wild, O., and Archibald, A.: Tropospheric ozone changes, radiative forcing and attribution to emissions in the Atmospheric Chemistry and Climate Model Intercomparison Project (ACCMIP), Atmos. Chem. Phys., 13, 3063–3085, https://doi.org/10.5194/acp-13-3063-2013, 2013.

Szopa, S., Naik, V., Adhikary, B., Artaxo, P., Berntsen, T., Collins, W. D., Fuzzi, S., Gallardo, L., Kiendler-Scharr, A., Klimont, Z., Liao, H., Unger, N., and Zanis, P.: Short-Lived

Climate Forcers, in: Climate Change 2021: The Physical Science Basis. Contribution of Working Group I to the Sixth Assessment Report of the Intergovernmental Panel on Climate Change, edited by: Masson-Delmotte, V., Zhai, P., Pirani, A., Connors, S. L., Péan, C., Berger, S., Caud, N., Chen, Y., Goldfarb, L., Gomis, M. I., Huang, M., Leitzell, K., Lonnoy, E., Matthews, J. B. R., Maycock, T. K., Waterfield, T., Yelekçi, O., Yu, R., and Zhou, B., Cambridge University Press, Cambridge, United Kingdom and New York, NY, USA, 817–922, https://www.ipcc.ch/report/ar6/wg1/downloads/report/IPCC_AR6_WGI_Chapter06.pdf (last access: 1 November 2022), 2021.

Thornhill, G. D., Collins, W. J., Kramer, R. J., Olivié, D., Skeie, R. B., O'Connor, F. M., Abraham, N. L., Checa-Garcia, R., Bauer, S. E., Deushi, M., Emmons, L. K., Forster, P. M., Horowitz, L. W., Johnson, B., Keeble, J., Lamarque, J.-F., Michou, M., Mills, M. J., Mulcahy, J. P., Myhre, G., Nabat, P., Naik, V., Oshima, N., Schulz, M., Smith, C. J., Takemura, T., Tilmes, S., Wu, T., Zeng, G., and Zhang, J.: Effective radiative forcing from emissions of reactive gases and aerosols – a multi-model comparison, Atmos. Chem. Phys., 21, 853–874, https://doi.org/10.5194/acp-21-853-2021, 2021.

Turner, A. J., Fung, I., Naik, V., Horowitz, L. W., and Cohen, R. C.: Modulation of hydroxyl variability by ENSO in the absence of external forcing, P. Natl. Acad. Sci. USA, 115, 8931–8936, https://doi.org/10.1073/pnas.1807532115, 2018.

Vasquez, K.: Cleaner pandemic air led to reduced lightning strikes worldwide, Eos, 103, https://doi.org/10.1029/2022EO220048, 26 January 2022.

Venter, Z. S., Aunan, K., Chowdhury, S., and Lelieveld, J.: COVID-19 lockdowns cause global air pollution declines, P. Natl. Acad. Sci. USA, 117, 18984–18990, https://doi.org/10.1073/pnas.2006853117, 2020.

Weber, J., Shin, Y. M., Staunton Sykes, J., Archer-Nicholls, S., Abraham, N. L., and Archibald, A. T.: Minimal climate impacts from short-lived climate forcers following emission reductions related to the COVID-19 pandemic, Geophys. Res. Lett., 47, e2020GL090326, https://doi.org/10.1029/2020GL090326, 2020.

Wild, O., Prather, M. J., and Akimoto, H.: Indirect long-term global radiative cooling from NO_x emissions, Geophys. Res. Lett., 28, 1719–1722, 2001.

Wild, O., Fiore, A. M., Shindell, D. T., Doherty, R. M., Collins, W. J., Dentener, F. J., Schultz, M. G., Gong, S., MacKenzie, I. A., Zeng, G., Hess, P., Duncan, B. N., Bergmann, D. J., Szopa, S., Jonson, J. E., Keating, T. J., and Zuber, A.: Modelling future changes in surface ozone: a parameterized approach, Atmos. Chem. Phys., 12, 2037–2054, https://doi.org/10.5194/acp-12-2037-2012, 2012.

Zhao, Y., Saunois, M., Bousquet, P., Lin, X., Berchet, A., Hegglin, M. I., Canadell, J. G., Jackson, R. B., Deushi, M., Jöckel, P., Kinnison, D., Kirner, O., Strode, S., Tilmes, S., Dlugokencky, E. J., and Zheng, B.: On the role of trend and variability in the hydroxyl radical (OH) in the global methane budget, Atmos. Chem. Phys., 20, 13011–13022, https://doi.org/10.5194/acp-20-13011-2020, 2020.